Simulation of ozone depletion in spring 2000 with the Chemical Lagrangian Model of the Stratosphere (CLaMS)

J.-U. Grooß,[1] G. Günther,[1] P. Konopka,[1] R. Müller,[1] D. S. McKenna,[1] F. Stroh,[1] B. Vogel,[1] A. Engel,[2] M. Müller,[2] K. Hoppel,[3] R. Bevilacqua,[3] E. Richard,[4] C. R. Webster,[5] J. W. Elkins,[6] D. F. Hurst,[6] P. A. Romashkin,[6] and D. G. Baumgardner[7]

Received 7 February 2001; revised 26 June 2001; accepted 16 September 2001; published 24 October 2002.

[1] Simulations of the development of the chemical composition of the Arctic stratosphere for spring 2000 are made with the Chemical Lagrangian Model of the Stratosphere (CLaMS). The simulations are performed for the entire Northern Hemisphere on four isentropic levels (400–475 K). The initialization in early February is based on observations made from satellite, balloon and ER-2 aircraft platforms. Tracer-tracer correlations from balloon-borne cryosampler (Triple) and ER-2 measurements, as well as tracer-PV correlations, are used to derive a comprehensive hemispherical initialization of all relevant chemical trace species. Since significant denitrification has been observed on the ER-2 flights, a parameterization of the denitrification is derived from NO_y and N_2O observations on board the ER-2 aircraft and the temperature history of the air masses under consideration. Over the simulation period from 10 February to 20 March, a chemical ozone depletion of up to 60% was derived for 425–450 K potential temperature. Maximum vortex-averaged chemical ozone loss rates of 50 ppb d^{-1} or 4 ppb per sunlight hour were simulated in early March 2000 at the 425 and 450 K potential temperature levels. We show comparisons between the measurements and the simulations for the location of the ER-2 flight paths in late February and March and the location of the Triple balloon flight. The simulated tracer mixing ratios are in good agreement with the measurements. It was not possible to reproduce the exact details of the inorganic chlorine compounds. The simulation agrees with ClO_x observations on the Triple balloon flight but overestimates for the ER-2 flights. The simulated ozone depletion agrees with estimates from other observations in the 425 and 450 K levels, but is underestimated on the 475 K level. *INDEX TERMS:* 0340 Atmospheric Composition and Structure: Middle atmosphere—composition and chemistry; 0341 Atmospheric Composition and Structure: Middle atmosphere—constituent transport and chemistry (3334); 0317 Atmospheric Composition and Structure: Chemical kinetic and photochemical properties; *KEYWORDS:* Stratosphere, ozone, ozone depletion, CLaMS, Lagrangian, denitrification

Citation: Grooß, J.-U., et al., Simulation of ozone depletion in spring 2000 with the Chemical Lagrangian Model of the Stratosphere (CLaMS), *J. Geophys. Res.*, *107*(D20), 8295, doi:10.1029/2001JD000456, 2002.

1. Introduction

[2] In winter 1999/2000 an extensive measurement campaign (SOLVE/THESEO-2000) was conducted with the aim of studying Arctic ozone loss in great detail. Measurements made from various platforms were collected giving the opportunity to examine the processes involved in Arctic ozone loss. Winter 1999/2000 was characterized by very low temperatures in the stratosphere with minimum temperatures below 185 K on the 525 K isentropic level in January and below 192 K on the 450 K isentropic level between mid February and mid March. In early February, stratospheric temperatures were higher [*Manney and Sabutis*, 2000]. Owing to these low temperatures, polar stratospheric clouds (PSCs) could form that are known to lead to the formation of active chlorine species from the chlorine reservoirs HCl and $ClONO_2$, thus causing chemical ozone depletion. The sedimentation of large PSC particles led to a pronounced denitrification and slight dehydration that were observed in situ during this winter [*Fahey et al.*, 2001; *Schiller et al.*, 2002]. Both the long duration of low stratospheric temperatures and the denitrification encourage extensive Arctic ozone depletion.

[1]Institute for Stratospheric Chemistry (ICG-1), Forschungszentrum Jülich, Germany.
[2]Institute for Meteorology, University of Frankfurt, Frankfurt, Germany.
[3]Naval Research Laboratory, Washington, DC, USA.
[4]Aeronomy Laboratory, NOAA, Boulder, Colorado, USA.
[5]Jet Propulsion Laboratory, California Institute of Technology, Pasadena, California, USA.
[6]Climate Monitoring and Diagnostics Laboratory, NOAA, Boulder, Colorado, USA.
[7]Centro de Ciencias de la Atmosfera, Universidad Nacional Autonoma de Mexico, Mexico City, Mexico.

0148-0227/02/2001JD000456

[3] The ozone mixing ratios measured on a variety of platforms in mid March inside the polar vortex were generally below 1.5 ppmv at the 450 K potential temperature level (about 19 km altitude), while in mid February typically about 2.8 ppm was observed confirming a substantial chemical ozone loss. *Sinnhuber et al.* [2000] performed a simulation with the SLIMCAT model and compared the results with data from the Global Ozone Monitoring Experiment (GOME). They found column ozone depletion of 90–140 Dobson units corresponding to about a 30% reduction of the total ozone column by the end of March.

[4] This study concentrates on the period from mid February to mid March 2000, where owing to low temperatures, denitrification and large fractions of sunlight conditions promoted significant chemical ozone depletion. The ozone depletion prior to this period is not investigated here. We present simulations with the Chemical Lagrangian Model of the Stratosphere (CLaMS) [*McKenna et al.*, 2002a, 2002b] and compare these with observations. The CLaMS model is described in section 2. Section 3 describes the measurements used in this study. The method used to derive the initialization on 10 February is explained in section 4. Section 5 contains the results of the simulation and a comparison with the measurements and other estimates of chemical ozone loss.

2. Model Description

[5] The Chemical Lagrangian Model of the Stratosphere (CLaMS) is a chemistry transport model that is described in detail by *McKenna et al.*, [2002a, 2002b]. It simulates the dynamics and chemistry of multiple air parcels along their trajectories. The trajectories are determined from European Centre for Medium-Range Weather Forecasts (ECMWF) wind fields. The interaction between neighboring air parcels (mixing) is introduced by both combining air parcels and adding new air parcels under certain conditions determined by the wind field [*McKenna et al.*, 2002a]. There are 36 chemical species and 114 chemical reactions implemented in the chemistry scheme. The development of the chemical composition of the air parcels is calculated by a solver routine based on the so-called family concept [*Carver and Scott*, 2000]. Photolysis frequencies are calculated by a scheme that solves the radiative transfer equation in spherical geometry [*Lary and Pyle*, 1991; *Becker et al.*, 2000a]. The absorption cross sections and reaction rate constants are taken from current recommendations [*DeMore et al.*, 1997; *Sander et al.*, 2000].

[6] PSC particle formation and heterogeneous reaction rates are calculated using a scheme developed by *Carslaw et al.* [1995]. Its use within CLaMS is described by *McKenna et al.* [2002b]. Briefly, the particle phases considered are liquid ternary $H_2SO_4/HNO_3/H_2O$ solution aerosols, solid sulfuric acid tetrahydrate (SAT), nitric acid trihydrate (NAT), and water ice particles. The supersaturation of HNO_3 over NAT leading to the formation of NAT particles is prescribed: normally a supersaturation of 10 corresponding to about 3 K supercooling is used. The NAT and ice particle size distribution is represented by a lognormal distribution. The number density of NAT particles of 1 cm^{-3} and ice particles of 0.01 cm^{-3} is assumed at the locations where the particles form.

[7] Sedimentation of these particles leads to the removal of HNO_3 and H_2O from the air masses under consideration, effects known as denitrification and dehydration, respectively. Being a reservoir for NO_x, the removal of HNO_3 intensifies and extends the chlorine activation period since the moderating effect of NO_x that causes the formation of inactive $ClONO_2$ is reduced. Because of the importance of denitrification during winter 1999/2000 a parameterization for the sedimentation of NAT and ice particles and the subsequent effect of HNO_3 and H_2O removal has been introduced into the model. Assuming spherical particles, the terminal settling velocity of the particles is computed [see, e.g., *Seinfeld and Pandis*, 1998] from the volumes determined by the microphysics scheme. From these terminal settling velocities the corresponding downward mass flux of HNO_3 and H_2O due to sedimentation is calculated assuming the air mass under consideration to be of a characteristic height. In the following simulations we assume the same characteristic height of 250 m for all air parcels considered, which yields NO_y consistent with ER-2 observations (see below). The choice of a lower characteristic height increases the simulated denitrification effect which is shown in a sensitivity study. In the present study we do not consider nitrification and hydration through PSC particles that sediment from above into the simulated air parcels.

[8] Here the simulations with CLaMS are performed in two different modes: (1) the CTM mode that is an isentropic simulation with mixing within the four isentropic levels (400, 425, 450, and 475 K) without interaction between the levels and (2) the pure advection mode that is a diabatic multiple box model simulation with pure advection and without mixing. The vertical motion due to the diabatic heat exchange of the air parcels with the radiation field, in particular the diabatic descent in the winter polar vortex, is calculated by a radiation scheme [*Morcrette*, 1991; *Zhong and Haigh*, 1995]. This pure advection mode is used to transform observations with varying time and location into a synoptic time (e.g., in the initialization) and also to transform the CLaMS results from a synoptic time to any time and location of interest (e.g., for a comparison between simulation and observation along a flight path). Both modes use the same trajectory and chemistry modules. The distinction between these modes is necessary since the mixing routine currently only calculates the interaction between air parcels within one isentropic level and cannot yet be applied for air parcels distributed arbitrarily in three-dimensional space. If only chemically inert tracers are considered, a pure advection calculation can be performed without chemistry using diabatic backward/forward trajectories from the observation locations and times to a synoptic time.

3. Observations

[9] The ER-2 is a high-altitude aircraft capable of flight altitudes of up to about 20 km. During the SOLVE/THESEO-2000 campaign it was based in Kiruna, Sweden (68°N, 20°E), from where scientific flights were carried out in two periods, seven flights from 14 January to 3 February and five flights from 26 February to 16 March. On board the ER-2 a payload of multiple instruments is installed that measure the chemical composition of the stratospheric air in situ.

[10] The dual-beam UV-absorption ozone photometer [*Proffitt and McLaughlin*, 1983] measures ozone with an accuracy of 3% and a time resolution of 1 Hz. The airborne chromatograph for atmospheric trace species (ACATS-IV) of National Oceanic and Atmospheric Administration/Climate Monitoring and Diagnostics Laboratory (NOAA/CMDL) [*Elkins et al.*, 1996; *Romashkin et al.*, 2001] measures seven halocarbons, N_2O, CH_4, SF_6, and H_2 using gas chromatography with electron capture detection at intervals of 70 or 140 s. Organic chlorine (CCl_y) and organic bromine (CBr_y) are determined for the sampled air masses by summing measurements of chlorinated and brominated source gases in the lower stratosphere by ACATS and the National Center for Atmospheric Research whole air sampler [*Schauffler et al.*, 1999]. The amounts of CCl_y and CBr_y in these air masses when they enter the stratosphere (total Cl and Br) are estimated from CO_2-derived mean ages and tropospheric trends of source gases monitored by CMDL. Inorganic chlorine and bromine (Cl_y and Br_y) are calculated as the difference between total Cl (Br) and CCl_y (CBr_y) for each sampled air mass.

[11] The NO_2-ClO-$ClONO_2$-BrO instrument [*Stimpfle et al.*, 1999] is composed of two parts: a laser-induced fluorescence instrument for the detection of NO_2 and a resonance fluorescence instrument for the detection of ClO and BrO that also has a thermal dissociation axis used for the detection of $ClONO_2$ and Cl_2O_2.

[12] The Aircraft Laser Infrared Absorption Spectrometer (ALIAS) instrument [*Webster et al.*, 1994] on board the ER-2 is a high time resolution scanning tunable diode laser spectrometer that makes direct, simultaneous measurements of HCl, CO, CH_4, and N_2O.

[13] The NO_y instrument [*Fahey et al.*, 1989] has three independent chemiluminescence detectors for simultaneous measurements of NO_y and NO. NO_y is the sum of all reactive nitrogen compounds that are reduced to NO by catalytic reduction on a gold surface with carbon monoxide acting as a reducing agent. There are two inlets that have very different sampling characteristics with respect to the aerosol particle size. Here the data from the rear inlet of the NO_y instrument are used. Due to flow dynamics, particles with a diameter larger than about 3 μm are not sampled by the inlet. NO_y-containing particles with a diameter below 3 μm are likely to be collected in higher concentration than in ambient air, which causes an enhancement of the NO_y signal [*Fahey et al.*, 1989].

[14] During the SOLVE/THESEO-2000 campaign a balloon-borne payload composed of three scientific instruments was flown on 27 January and 1 March 2000. The instruments on this Triple payload include the fast in situ hygrometer [*Schiller et al.*, this issue], the ClO instrument [*Vogel et al.*, 2002; *Pierson et al.*, 1999], and a cryogenic whole air sampler [*Schmidt et al.*, 1987]. In this study, the measurements of the ClO instrument and the whole air sampler are used. The ClO instrument utilizes the chemical-conversion resonance-fluorescence technique [*Brune et al.*, 1989]. The whole air samples are collected cryogenically in evacuated and conditioned sample bottles cooled with liquid neon and are analyzed by gas chromatography using an electron capture detector. The vertical profiles of the most important CFC species for calculating the chlorine budgets, as well as SF_6 and N_2O, were obtained from these measurements.

[15] Data from two satellite experiments were also used in this study. The Halogen Occultation Experiment (HALOE) on UARS [*Russell et al.*, 1993] and the Polar Ozone and Aerosol Measurement (POAM-3) on SPOT-4 [*Lucke et al.*, 1999] are both satellite experiments that measure ozone and other species using the solar occultation technique. They observe daily profiles at multiple longitudes along two latitude circles determined by the satellite's orbit. POAM-3 observes 14 sunrise profiles per day around 65°N. HALOE observes 15 sunrise and 15 sunset profiles per day at lower latitudes; the maximum latitude is 56°N in February and in 63°N mid March. In winter 1999/2000, vortex observations by HALOE prior to early March are rare.

4. Initialization Procedure

[16] The CLaMS simulation described here starts on 10 February 2000 and is performed on four isentropic levels (400, 425, 450, and 475 K). The horizontal resolution (i.e., the average distance between an air parcel and its next neighbors) is about 90 km. To derive an initialization for the entire Northern Hemisphere that is as realistic as possible, a complex procedure is used similar to the initialization for winter 1996/1997 described by *McKenna et al.* [2002b]. The idea of this procedure is to combine multiple available data sets that have very different accuracy and coverage into a hemispheric initialization for one particular time (10 February 2000). To account for the different availability of data for the chemical species, different methods are used to initialize the simulation.

4.1. O_3

[17] The initialization of ozone is taken from the multiple data sources. The air masses sampled by HALOE and POAM-3 within ±7 days of 10 February within ±7 days of 10 February were transformed into their corresponding locations by a pure advection calculation. The chemical ozone destruction along these trajectories is not taken into account here due to the lack of more accurate information on the chemical composition of these air masses. However, typically the expected ozone depletion under the relatively dark early February conditions within 7 days should stay within the data accuracy (2σ). The third data source for ozone is the observations made on board the ER-2 between 14 January and 3 February. The air parcels sampled by ER-2 were followed to their corresponding locations on 10 February. Ozone depletion in these air masses was taken into account by a CLaMS integration in the pure advection mode. The simulation was performed for air parcels every 10 s of the flight tracks of all seven ER-2 flights between 14 January and 3 February. The corresponding trajectories were initialized by the chemical composition measured by the ER-2. Species not measured by the ER-2 are taken from the Mainz photochemical two-dimensional (2-D) model [*Gidel et al.*, 1983; *Grooß*, 1996]. The species within the chemical families Cl_y, Br_y, and NO_y were scaled linearly in order to match the measured family sum. With this simulation the chemical composition of the air masses sampled by ER-2 (i.e., about 12,000 air parcels) on 10 February is simulated taking into account diabatic descent and ozone depletion. From all the air parcels, only those were selected that are within ±3 K of the isentropic levels of the

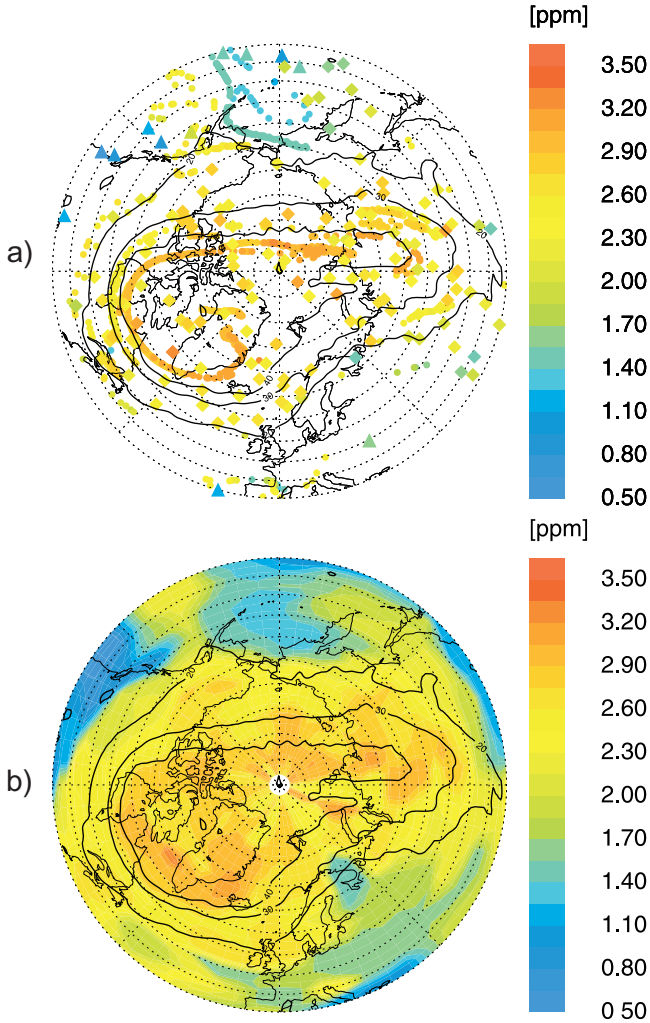

Figure 1. Ozone initialization on 10 February 2000 for the θ = 450 K level. (a) Locations of air parcels observed by ER-2 (circles), POAM (diamonds), and HALOE (triangles) that have been advected to the initialization date (see text). The symbols are color-coded by the ozone mixing ratio. (b) Hemispheric ozone field derived from these data. The PV contours 20, 30, and 40 PVU are overlaid as black lines.

simulation. Figure 1a shows the ozone mixing ratios derived in this way on 10 February at the location of all air masses sampled by HALOE, POAM, and ER-2 at the 450 K level. These data points are combined into a regular 3-D grid by using cosine-square weighting with 6 degrees half-width in longitude and 2 degrees half-width in latitude weighted by the individual measurement accuracy. Where no data were available, the data were interpolated from the neighboring grid cells. Figure 1b displays the derived hemispherical ozone field from these data.

4.2. CH_4

[18] To initialize the chemically inert tracer CH_4, a different procedure was employed since a lower coverage of CH_4 data is available than that of O_3 data. Data from HALOE, ER-2, and the cryogenic whole air sampler on board the Triple balloon were used. No HALOE data within the polar vortex are available prior to 19 February 2000, and no ER-2 data are available for the 475 K level. Therefore the available data were analyzed for a later time point 25 February. The air masses sampled by HALOE within ±7 days of 25 February, the ER-2 ALIAS measurements from 26 February and the cryogenic whole air sampler measurements from 1 March were transformed to the synoptic time point 25 February by a pure advection calculation. As an example, Figure 2 shows these data as a function of equivalent latitude for the 450 K isentrope. A tight correlation of the CH_4 data with equivalent latitude is found on all four simulation levels and is approximated by a spline fit (red line). This correlation is considered to be representative of the Northern Hemisphere on 25 February and is mainly changed by diabatic descent inside the polar vortex. We used this correlation here to initialize CH_4 from the equivalent latitude derived from the ECMWF analysis for 10 February. Through this procedure we also compensate for the neglect of diabatic descent during the first 2 weeks of the simulation period.

4.3. N_2O, Cl_y, Br_y

[19] Tracer correlations have been studied for all measurements at mid latitudes to high latitudes made by ACATS (ER-2) and by the cryogenic whole air sampler (Triple). Figure 3 shows that these correlations are very tight, even though the ER-2 measurements mainly constitute horizontal scans and the Triple balloon constitutes vertical profiles. With polynomial fits to these data (see Table 1) the CH_4 initialization was used to determine the mixing ratios of N_2O, total inorganic chlorine (Cl_y), and total inorganic bromine (Br_y).

4.4. NO_y

[20] The total inorganic nitrogen species (NO_y) cannot be initialized using a tracer correlation relation in a similar manner, since sedimentation of the HNO_3-containing PSCs caused by the low temperatures in mid January to early

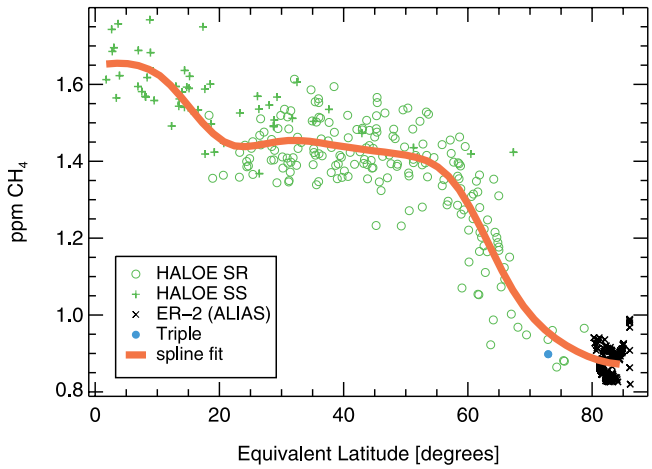

Figure 2. CH_4 data as a function of PV on the 450 K isentrope. The green symbols show the HALOE sunrise (circles) and sunset (pluses) data between 19 February and 4 March. The black crosses show ER-2/ALIAS data from the 26 February flight. All data are transformed to their location on 10 February by an advection calculation (see text). The red line shows a spline fit to this correlation that is used in the initialization procedure.

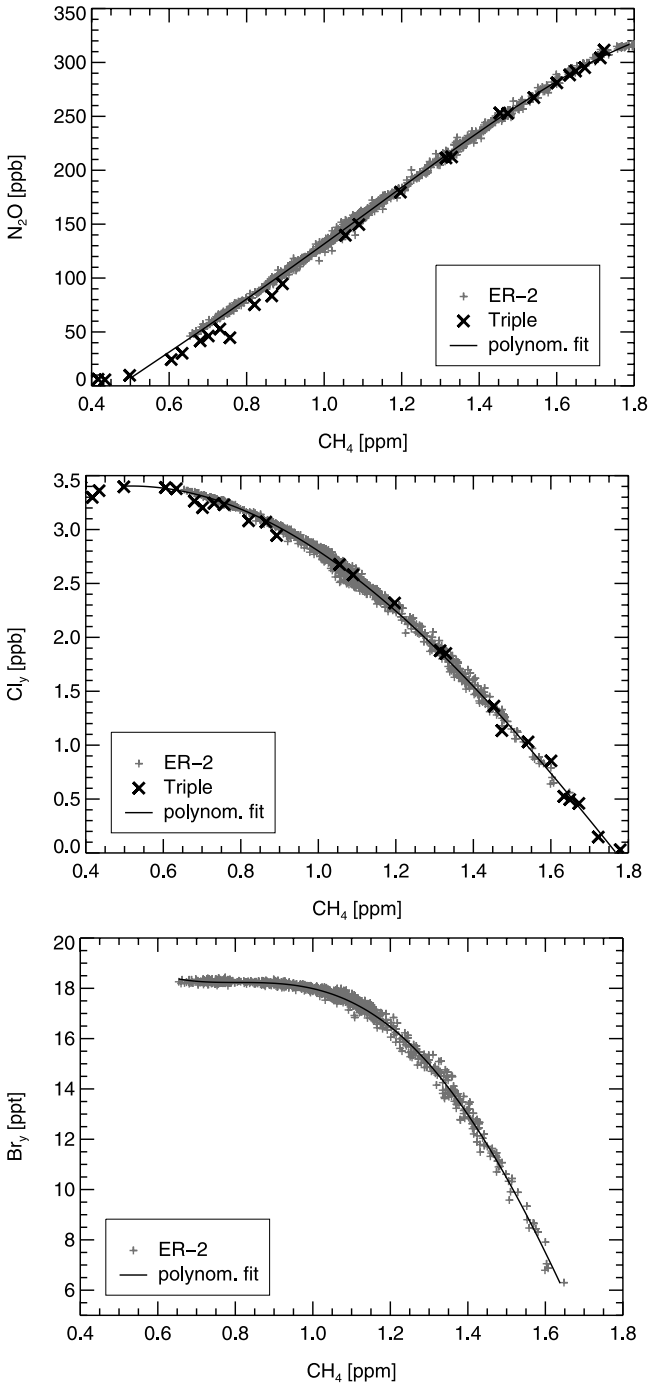

Figure 3. Tracer/tracer correlations. Shown are the correlations between CH_4 and (top) N_2O, (middle) Cl_y, and (bottom) Br_y measured by the ACATS instrument on all ER-2 flights between 20 January and 12 March (gray symbols) and by the whole air sampler on two balloon flights on 27 January and 1 March (black symbols) with the Triple gondola. Also shown is a fourth-order polynomial fit to these data that is used in the initialization procedure.

February destroys the tight correlation that is observed under unperturbed conditions. To estimate the extent of denitrification, an auxiliary CLaMS simulation in the pure advection mode was performed for the time period from 8 January through 10 February. The endpoints are a regular grid of 1.5° latitude and 4° longitude on each of the four isentropic levels. For this auxiliary simulation (hereinafter simulation A), NO_y was initialized using an unperturbed N_2O/NO_y relation from prewinter measurements from MkIV and ER-2 [*Popp et al.*, 2001]. The other tracers of simulation A (CH_4, N_2O, Cl_y, and Br_y) were initialized in the same way as above for 10 February. All other species (including ozone) were taken from the Mainz 2-D model. The denitrification is then calculated from the parameterization described above using different characteristic height and NAT particle number density. A characteristic height of 250 m and a NAT number density of 1 cm^{-3} resulted in good agreements with later NO_y observations (see below). The sensitivity to the choice of these parameters is also shown below. The NO_y on the regular grid on 10 February derived in this way is then interpolated to the locations of the air parcels.

4.5. Chlorine Partitioning

[21] The partitioning within the inorganic chlorine species, in particular the ratio between active chlorine species and chlorine reservoirs on 10 February, was also determined by the auxiliary simulation A discussed above. From that simulation the degree of chlorine activation $(ClO+2\cdot Cl_2O_2)/Cl_y$ is determined and then interpolated onto the locations of the air parcels. The inorganic chlorine species are scaled individually such that the sum Cl_y remains unchanged. With this method, the Cl_y/CH_4 relation corresponds to the observations and the chlorine activation corresponds to the simulation. Measurements of the individual inorganic chlorine compounds are not used in this context.

4.6. Other Species

[22] The remaining chemical species are of less importance for the chemical simulations and are initialized using the Mainz 2-D photochemical model results [*Gidel et al.*, 1983; *Grooß*, 1996]. These are mapped onto the equivalent latitude to account for the nonzonal vortex shape.

5. Simulation

[23] The simulation was performed for the period from 10 February to mid March on four isentropic levels (400, 425, 450, and 475 K). The reason for choosing isentropic levels is that during the simulation period the vertical displacement inside the vortex due to diabatic descent is small. Diabatic trajectory simulations indicate diabatic vertical displacements of only ±10 K within the polar vortex and ±25 K in midlatitudes between 10 February and 15 March on all simulation levels. Part of the diabatic displacement is compensated by the initialization procedure for CH_4 and thus for the other inert tracers as explained above. The horizontal resolution is about 90 km corresponding to approximately 25,000 points per level. The wind data are taken from the ECMWF analysis. The critical Lyapunov exponent λ_c that determines the strength of mixing was set to 1.2 d^{-1} and the mixing time step is 24 hours. These parameters give the best representation of mixing on the basis of tracer studies [*Konopka et al.*, 2002].

[24] The vortex-averaged ozone depletion rates for each isentropic level were calculated for each day of the simulation. The vortex edge was defined by the criterion of *Nash*

Table 1. Tracer Correlations Used in the Initialization Procedure

[x], ppm	[y]	Valid Range of [x], ppm	a_0	a_1	a_2	a_3	a_4
CH_4	N_2O, ppb	0.50 .. 1.81	−124.9	311.9	−158.1	146.6	−43.92
CH_4	Cl_y, ppb	0.48 .. 1.78	2.624	3.086	−3.156	0.147	0.100
CH_4	Br_y, ppt	0.65 .. 1.64	44.30	−106.3	155.0	−92.83	17.80

The tracer correlations are derived from the observations using a polynomial fit of the form $[y] = \Sigma_{i=0}^{n} a_i \cdot [x]^i$ and degree $n = 4$.

et al. [1996] averaged between 10 February and 11 March corresponding to PV values 17.2, 23.1, 33.5 and 42.4 PVU for the isentropic levels 400, 425, 450, and 475 K, respectively. The vortex-averaged ozone depletion rates are shown in Figure 4 both as ozone depletion per day and ozone depletion per sunlight hour. To calculate the latter rates, sunlight is assumed for all times with solar zenith angles below 95°. While in the top and bottom simulation levels (475 and 400 K) the simulated ozone depletion rates are moderate, the simulation yields a chemical ozone loss rate of about 50 ppb d^{-1} peaking in early March. The determination of this vortex-averaged ozone depletion rate is sensitive to the choice of the polar vortex edge. Especially in March, a weaker vortex criterion than was used by *Rex et al.* [2002] leads to 20–30% lower ozone depletion rates. In the first half of March significant ozone depletion was simulated but only over a limited vertical extent. Although the ozone depletion rates per sunlight hour are not very large (3–4 ppbv d^{-1}), more sunlight is available during March, and thus significant ozone depletion occurs.

[25] To determine the accumulated chemical ozone loss over the simulation period, also a hypothetical passive ozone tracer was initialized equally to the real ozone and was transported without any chemical change. The difference from the simulated ozone is then a measure of the chemical ozone depletion of the simulation. Figure 5 shows the chemical ozone change between 10 February and 15 March on the 450 K isentrope. Within the polar vortex core region ozone has been depleted by up to 1.8 ppm (≈60%) since 10 February. Figure 6 shows the simulated chemical ozone loss for the four levels averaged over equivalent latitude bins. The simulated ozone loss increases from the vortex edge toward the vortex core region. The largest ozone loss, about 1.6 ppm, is found above 80° equivalent latitude. Figure 6 also shows why the vortex-averaged ozone depletion is sensitive to the choice of the polar vortex edge.

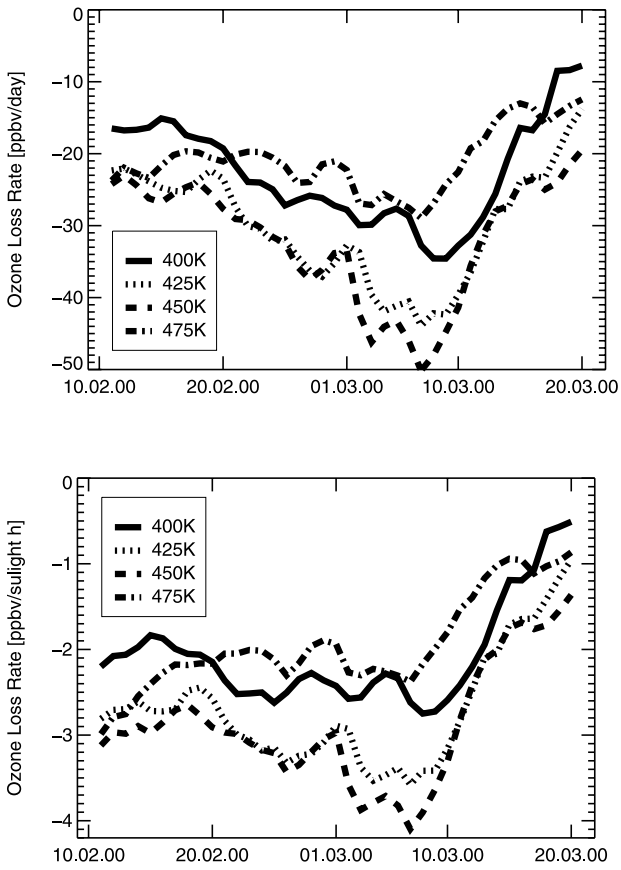

Figure 4. Simulated ozone change rates averaged over the polar vortex as a function of time for the four simulation levels given in ppbv d^{-1} (top) and ppbv per sunlight hour (bottom).

5.1. Comparison With Other Ozone Loss Estimates

[26] Other studies also have determined ozone loss rates for winter 1999/2000. *Richard et al.* [2001] derived ozone loss rates from the change of ozone/tracer correlations between 3 February and 12 March observed by the ER-2.

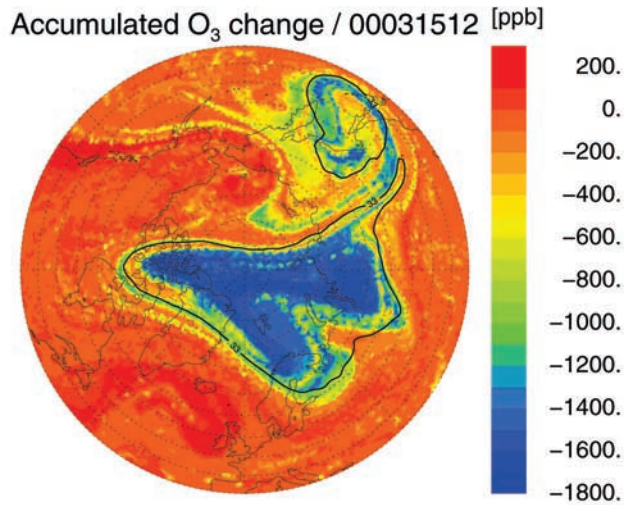

Figure 5. Results of the simulation for 15 March 2000. Shown is the chemical ozone change since 10 February 2000 on the 450 K isentropic level. The thick black line marks the potential vorticity of 33 PVU that approximately corresponds to the vortex edge.

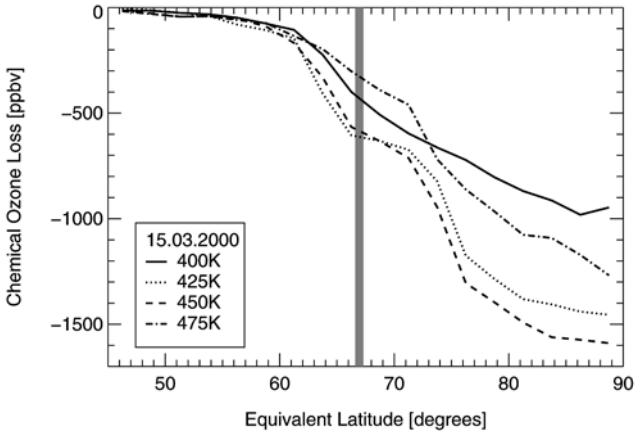

Figure 6. Results of the simulation for 15 March 2000. Shown is the chemical ozone change since 10 February 2000 averaged over equivalent latitude bins for the different simulation levels. The vertical bar corresponds to the equivalent latitude of the vortex edge used in Figure 4.

On the 400, 425, and 450 K levels they deduce an ozone depletion of about 20, 33 and 46 ppb d^{-1}, respectively. To compare these results with our simulations, we average the ozone depletion rates shown in Figure 4 over the period up to 12 March. The corresponding vortex-averaged ozone depletion rates are 25, 32, and 34 ppb d^{-1}, while an average over the vortex core region only (equivalent latitude >80°) yields 29, 46, and 47 ppb d^{-1} on the three levels, respectively. The ozone depletion rates on the 425 and 450 K levels estimated by *Richard et al.* [2001] are a composite of vertical profiles observed in the vortex core (during a ''dive'' maneuver) and toward the vortex edge (near takeoff and landing). For those levels the simulated ozone depletion averaged over the vortex agrees better with the estimate by *Richard et al.* [2001]. On the 450 K level the estimate agrees with the results of the simulation averaged over the vortex core region only.

[27] *Rex et al.* [2002] use the Match technique to determine ozone loss rates from multiple ozone soundings. They determine a time-dependent ozone depletion rate averaged over the polar vortex. Both for Match and the simulation, between 400 and 475 K the maximum ozone depletion rate is found in early March. The maximum Match ozone depletion rate, around 50 ppb d^{-1}, is found on the 450 K level. This was reproduced by the simulation. On the 425 K level both Match and the CLaMS simulation agree with a peak ozone loss rate of around 45 ppb d^{-1}. On the 475 K level the agreement between the simulation and Match analysis is poorer: the peak Match ozone loss rate in early March (40 ppb d^{-1}) is underestimated by about 30–35%. However, when using the vortex definition of *Rex et al.* [2002], the vortex average of the simulated ozone loss rates on the 425 and 450 K levels of the simulation is about 20–30% lower, pointing to an underestimation of ozone depletion in the vortex edge region on these levels as well.

[28] The simulated accumulated chemical ozone loss was also compared with estimates from other sources. *Robinson et al.* [2002] determine chemical ozone loss with the tracer correlation method from balloon observations between late January and early March (Dirac and Descartes experiments corresponding to 4 and 7 March, respectively). We compare these estimates to the CLaMS results in the vortex core of the corresponding days. In the 425 and 450 K levels the simulated ozone loss is about 0.3 ppm lower than these values. Assuming that ozone was destroyed at a rate of about 22 ppb d^{-1} between late January and 10 February, the start of the simulation (in accordance with the Match results), the difference can be explained. On the 475 K level the difference is about 0.6 ppm, which is more than expected. *Hoppel et al.* [2002] derive the vortex-averaged chemical ozone loss for 15 March from POAM-3 observations in combination with a passive tracer from a CTM (SLIMCAT). We compare these values to our vortex averages for the same day. In the 425 and 450 K levels the simulated chemical ozone depletion is 0.3 and 0.4 ppm lower than the POAM estimates. As above, this difference is likely due to chemical ozone depletion in early winter prior to the simulation period. On the 475 K level, the simulated ozone depletion is 0.9 ppm lower than the POAM estimate. In summary, the simulated ozone loss in the 425 and 450 K levels agrees well with that derived from observations. On the 475 K level the model seems to systematically underestimate ozone loss. In the following sections the CLaMS simulation is directly compared to observations of various trace species.

5.2. Comparison With ER-2 Measurements

[29] The simulations were compared with the measurements taken on board the ER-2 aircraft that had five flights out of Kiruna within the simulation period (26 February, 5, 7, 11, and 12 March). Both chemically inert tracers and photochemically active species are compared along the ER-2 flight track. For this purpose a CLaMS integration in the pure advection mode was performed from the last CLaMS output time step (previous day 1200 UTC) to the ER-2 flight track in time and space. With this method, the effect of the diurnal cycle of photochemically active species is accounted for.

[30] Figures 7 to 9 summarize the comparison of measurements and simulations for the ER-2 flight track for two flights inside the polar vortex, on 26 February and 12 March, which are the first and last flights within the simulation period. Figures 7 and 8 show the comparison as a function of time, while Figure 9 shows the vertical dependence for the 12 March flight. Only data above the 400 K isentropic level are shown. Between 1200 and 1230 UTC on 26 February and between 1330 and 1400 UTC on 12 March the plane performed a dive from the flight level down to below 400 K. The typical cruising altitude corresponds to about 430-460 K potential temperature.

5.2.1. CH_4 and Other Tracers

[31] The comparison between observations (ALIAS) and simulation results for CH_4 for the 26 February flight is generally very good. Near the vortex edge at 0815 UTC a filament of probably outside vortex air has not been simulated. The simulation overestimates the CH_4 mixing ratio by 0.1–0.2 ppm at the end of the flight on 12 March (i.e., above 450 K), a problem that is probably mostly due to the neglect of diabatic descent in the simulations. This shows that the tracer initialization and transport in the vortex is simulated well, at least below 450 K. The tracer structures across the vortex edge are also well resolved by

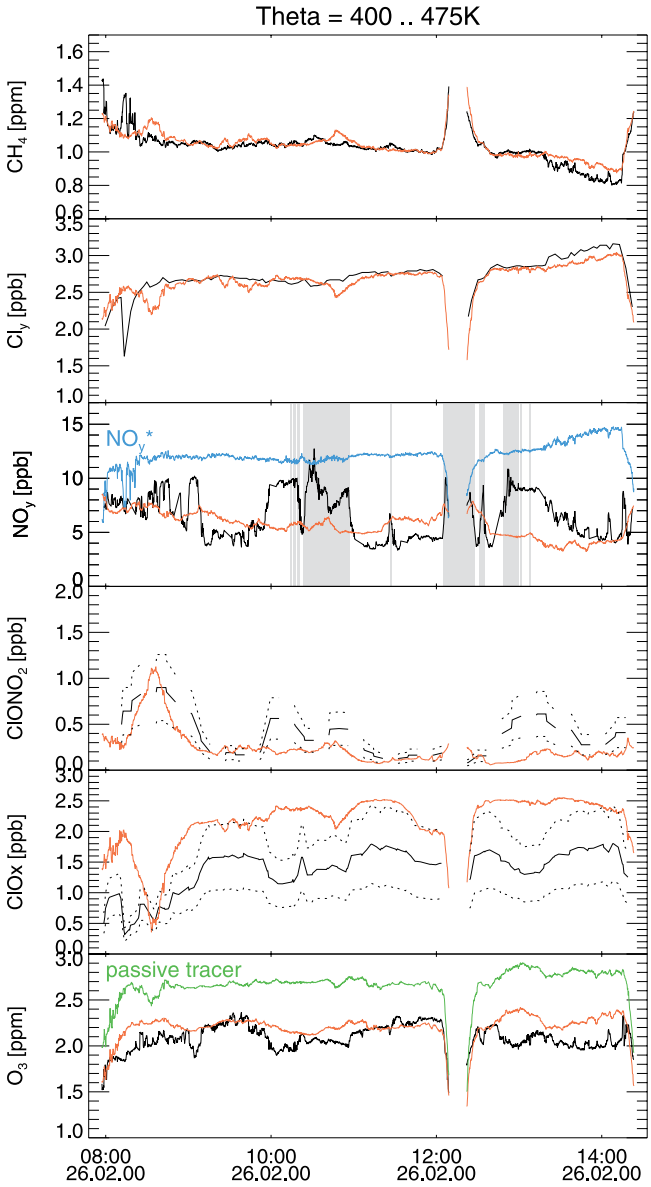

Figure 7. Comparison between ER-2 measurements and CLaMS simulations for the location of the ER-2 flight on 26 February 2000. The ER-2 data are shown as black lines and CLaMS simulations are shown as red lines. In the second panel also the NO_y* derived from measured N_2O is plotted in blue. The gray-shaded area depicts times when MASP aerosol volume density for particles below 3 μm diameter is above 0.5 μm^3 cm^{-3}. The simulated passive ozone tracer is plotted in the bottom panel as a green line. For $ClONO_2$ and ClO_x (=ClO + 2·Cl_2O_2) the accuracy of the data is shown by the dotted lines.

CLaMS including the small-scale filaments that are vortex remnants partially mixed with midlatitude air [see *Konopka et al.*, 2002]. Due to the close relationship between CH_4 and other chemically long-lived tracers (e.g., N_2O, Cl_y), the comparison between these tracer measurements and the simulation show very similar results. In particular, the comparison for Cl_y mirrors the comparison for CH_4.

5.2.2. NO_y

[32] Total reactive nitrogen (NO_y) is affected by denitrification caused by the sedimentation of the PSC particles. In the simulation, the major fraction of denitrification was found to be due to the sedimentation of NAT particles throughout January (simulation A). In the 450 and 475 K levels a denitrification of about 50 to 75%, in the 425 K level 20 to 50% and in the 400 K level less than 20% denitrification was simulated in the polar vortex by 10 February. The additional denitrification during the simulation period beginning on 10 February is lower owing to

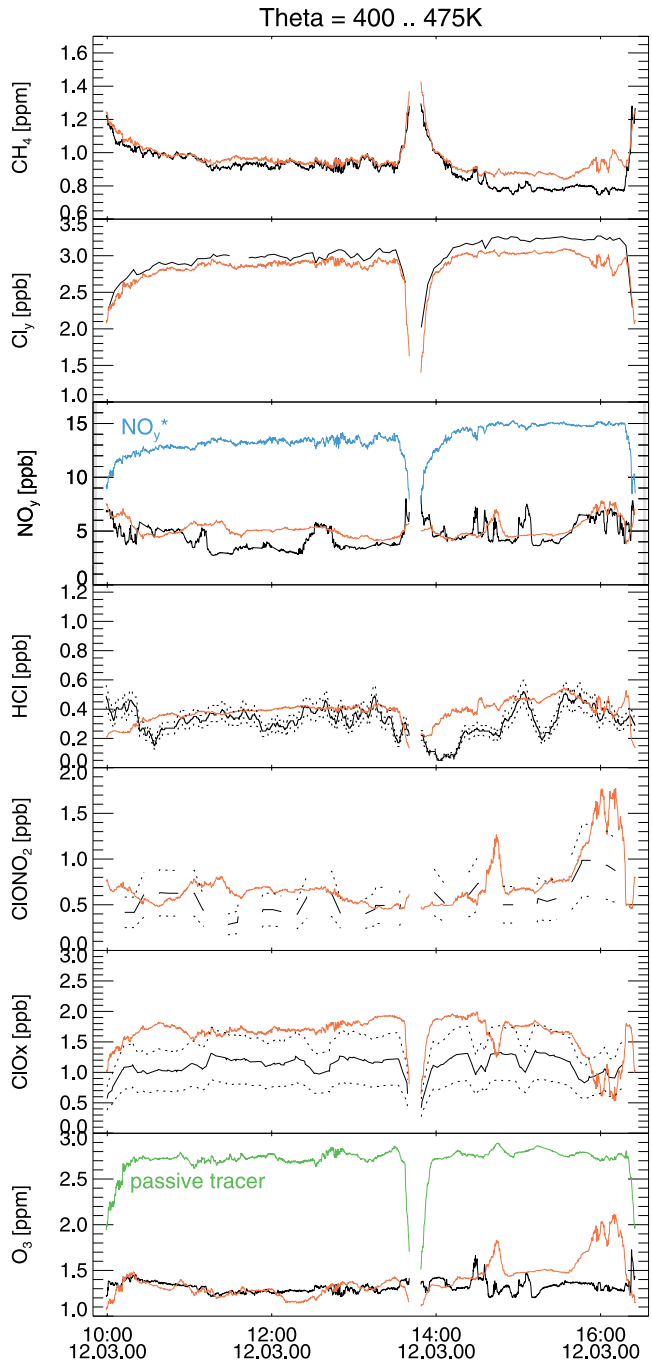

Figure 8. As Figure 7, but for the flight on 12 March 2000. For this flight, HCl data are also available.

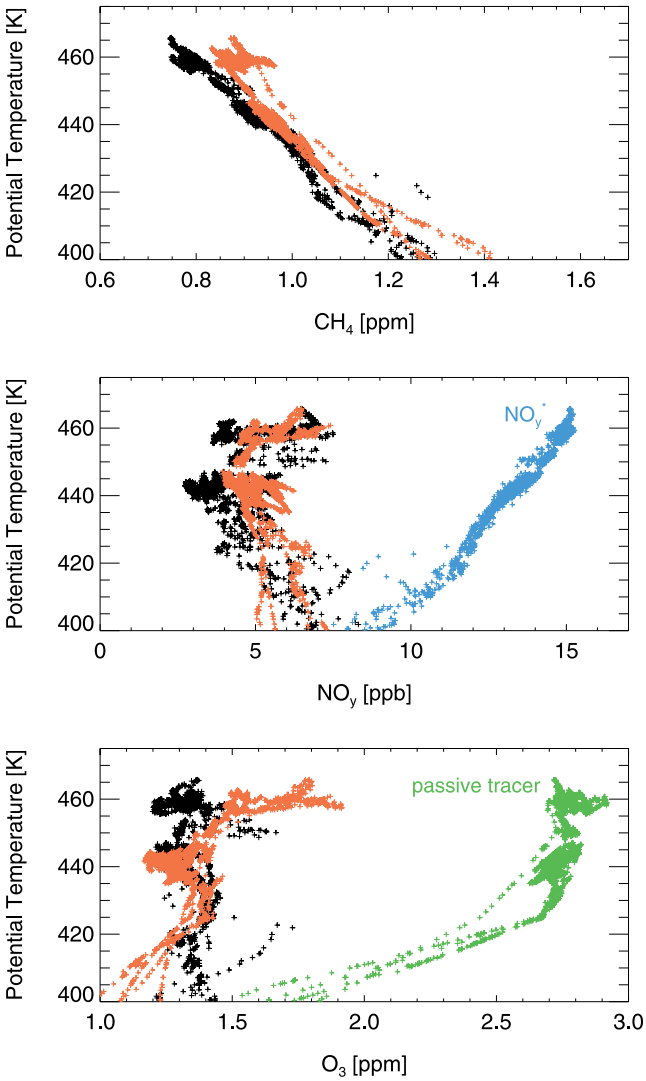

Figure 9. Vertical comparison between ER-2 measurements (black) and CLaMS simulations (red) for the location of the ER-2 flight on 12 March 2000. The data are depicted as a function of potential temperature. NO_y and the passive ozone tracer are displayed as in Figure 7.

higher stratospheric temperatures during this period. The settling velocities of NAT PSCs may be too low since much larger NAT particles have been observed [*Fahey et al.*, 2001]. Since the formation mechanism for these large NAT particles is yet unclear, no attempt is made here to simulate these particles. Rather, a comparison with measured NO_y on the flight track is made to verify that the simulated amount of denitrification is in accordance with the NO_y measurements. Figures 7 to 9 also show the measured and simulated NO_y. The blue line depicts NO_y*, which is the expected amount of NO_y derived from the N_2O data using the prewinter NO_y/N_2O correlation. NO_y* should be equal to NO_y in the absence of vertical redistribution through sedimentation. On 26 February the gray-shaded area indicates time periods for which particles below 3 μm diameter were observed by the MASP instrument corresponding to a volume above 0.5 μm^3 cm^{-3}. These particles are likely PSCs that cause an enhancement in the NO_y signal in the rear inlet. Therefore such time periods are not interpreted here. On 26 February there are large deviations that may be due to inaccuracies of the sedimentation routine. But the effect of enhancement of small PSC particles in the NO_y data would also be a possible explanation since during the flight the observed temperatures were below the NAT-existence temperature between about 0945 and 1415 UTC. However, a quantitative investigation of PSC size distribution and enhancement in the NO_y data is well beyond the scope of this study. Nevertheless, with respect to ozone depletion, the extent of denitrification starts to become important at the time when PSCs disappear. Although clearly PSC formation and sedimentation is not implemented in sufficient detail in the simulation to describe fine scale NO_y variations during periods of PSC occurrence, the magnitude of denitrification is approximately correct for 12 March when no PSCs were present. A sensitivity calculation was conducted to investigate the effect that different levels of denitrification may have on the simulated ozone depletion (see below).

5.2.3. Inorganic Chlorine Species

[33] During the first half of March, chlorine deactivation begins and the chlorine reservoirs $ClONO_2$ and HCl are reformed through the reactions $ClO+NO_2$ and $Cl+CH_4$. The major pathway for deactivation is the formation of $ClONO_2$. The denitrification causes very low values of NO_x within the vortex (<0.1 ppb on all ER-2 flights consistent with the simulation) which thus considerably slows down the process of chlorine deactivation. Figures 7 and 8 show the comparison of HCl (only 12 March), $ClONO_2$, and ClO_x (=$ClO + 2{\cdot}Cl_2O_2$). The dotted lines depict the uncertainty range of the data. The simulated active chlorine mixing ratio overestimates the measurements systematically by slightly more than the measurement accuracy. This is seen in all five ER-2 flights between 26 February and 12 March. The chlorine reservoir species are approximately reproduced within their uncertainty. The cause of these discrepancies cannot only be related to the simulations presented here. The sum of all measured inorganic chlorine species on board the ER-2 underestimates the ACATS Cl_y on the same flights by about 20% on average. This problem is still under investigation (D. Wilmouth et al., manuscript in preparation, 2001). Since the simulation is consistent with ACATS Cl_y, it cannot be consistent with all measured chlorine species simultaneously.

5.2.4. Ozone

[34] The comparison of simulated and observed ozone is given in the bottom panel of Figures 7 and 8. The green line shows the simulated passive ozone tracer values interpolated onto the ER-2 flight track. The difference from the simulated ozone is the chemical ozone loss. On 26 February the simulated ozone depletion along the ER-2 flight track (since 10 February) is about 0.6 ± 0.1 ppm. The simulated and observed ozone data agree better for the first part of the flight. A discrepancy of up to 0.35 ppm toward the end of the flight is found when the ER-2 was flying at higher altitudes. This higher ozone depletion may be either due to an inconsistent initialization or an underestimation of the ozone depletion in the simulations as was also found for this time of the year in earlier studies [e.g., *Woyke et al.*, 1999; *Becker et al.*, 2000b].

[35] For 12 March, CLaMS simulation of ozone and observations agree very well below the 450 K level. The

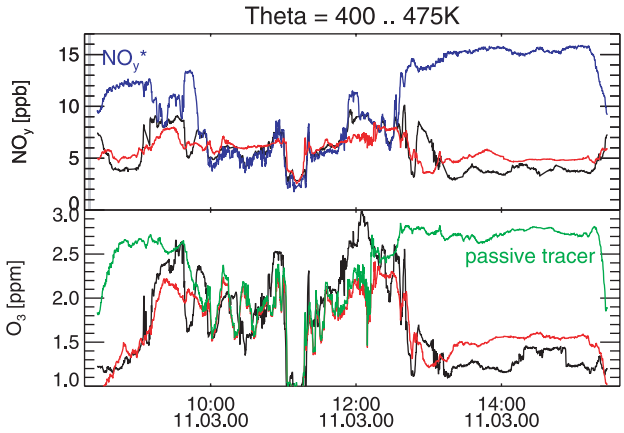

Figure 10. Comparison of O_3 and NO_y from ER-2 measurements and from CLaMS simulations for the location of the ER-2 flight on 11 March 2000 that crossed the vortex edge. Line colors are as in Figure 7.

comparison with the passive ozone tracer suggests a correct simulation of chemical ozone depletion at these altitudes. Above 450 K (at the end of the flight near 1600 UTC), CLaMS underestimates the ozone depletion on 12 March but part of this discrepancy was already seen on 26 February. Especially at the higher altitudes, the discrepancy may be due to a problem that was already identified in previous winters at the 475 K level and above [e.g., *Hansen et al.*, 1997; *Woyke et al.*, 1999; *Becker et al.*, 2000b]. However, with a systematically lower amount of active chlorine as measured on board the ER-2, the simulated ozone depletion would be even lower, and therefore the agreement between simulated and observed ozone may be worse.

5.2.5. Comparison of the Flight Through the Vortex Edge

[36] On 11 March the ER-2 aircraft undertook a flight that crossed the edge of the polar vortex and stayed outside the vortex between about 1000 and 1200 UTC. Figure 10 shows NO_y and ozone for that flight. In the stratosphere, both ozone and NO_y have long lifetimes in the absence of PSCs and active chlorine as is the case outside the polar vortex. Thus here the ozone and NO_y mixing ratios are determined by initialization and tracer transport only. The comparison of ozone and NO_y data with the CLaMS simulation outside the polar vortex shows very good agreement indicating a good quality of initialization outside the polar vortex. Even most of the filamentary structure at the vortex edge is reproduced in the simulation (see also *Konopka et al.* [2002]). The part of the flight inside the vortex is similar to the vortex flights described above.

5.3. Sensitivity With Respect to Denitrification and Particle Formation Assumptions

[37] To study the effect of different sedimentation parameterizations on the simulated results, sensitivity calculations were made (with a lower spatial resolution of about 200 km). Figure 11 displays a comparison of the simulated NO_y with that observed on 12 March for different assumptions. The reference simulation with an assumed characteristic height of 250 m and NAT particle number density of 1.0 cm^{-3} (red solid line) represents approximately an upper limit of NO_y. An additional CLaMS simulation (including the auxiliary simulation A) was performed, for which the assumed NAT number density was set to 0.1 cm^{-3}. The comparison with the ER-2 measurements (red dotted line) shows that this simulation represents roughly a lower limit of the observed NO_y. The variability of NO_y could not be reproduced by any of the simulations. Similar results were obtained by a simulation with a NAT particle density of 1 cm^{-3} in which the assumed characteristic height was lowered to 100 m. Figure 11 (bottom) shows that this changes the simulated ozone loss by less than 0.1 ppm. This result is also found for the other ER-2 flights. The red dashed line in Figure 11 corresponds to a third simulation for which denitrification was not taken into account. Here the simulated NO_y is almost congruent with the NO_y* derived from the ER-2 N_2O data. In this simulation, the peak ozone depletion rates in early March are 20% below the reference simulation. Starting in early March, also a more rapid chlorine deactivation and thus less ozone depletion was determined. The comparison of the simulated inorganic chlorine species with ER-2 data also shows no agreement for the no-denitrification case since chlorine deactivation caused $ClONO_2$ to be about 80% of the Cl_y on 12 March and thus much greater than observed (not shown). The simulated ozone depletion without denitrification along the 12 March flight track is about 0.1–0.25 ppm lower than in the reference case.

[38] Furthermore, by 20 March, in the vortex core the denitrification resulted in 0.3 ppm higher ozone depletion in the 450 K level (Figure 12). This demonstrates the significant influence of denitrification on ozone depletion in late winter. The effect of particle formation mechanisms was also investigated. Figure 12 (dotted line) displays the

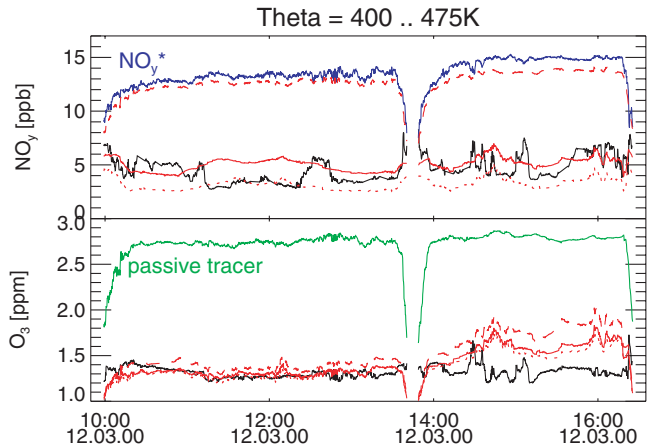

Figure 11. Sensitivity to the parameterization of sedimentation. As in Figure 8, CLaMS simulations and ER-2 measurements for ozone and NO_y are shown. The solid red line shows the the reference simulation (NAT particle density 1 cm^{-3}), the dotted red line shows a simulation with higher denitrification (NAT particle density 0.1 cm^{-3}), and the dashed line corresponds to a simulation without denitrification. (top) The NO_y* derived from ER-2 N_2O is plotted in blue. (bottom) The simulated passive ozone tracer is plotted as a green line.

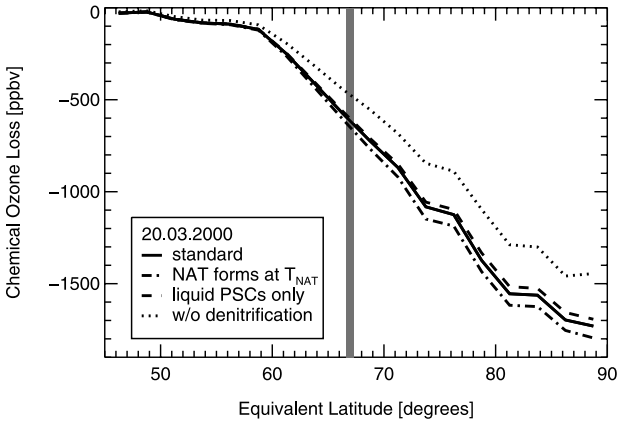

Figure 12. Sensitivity to denitrification and PSC formation assumptions, for 20 March 2000. Shown is the chemical ozone change since 10 February 2000 averaged over equivalent latitude bins for $\theta = 450$ K. The vertical bar corresponds to the equivalent latitude of the vortex edge used in Figure 4. The solid line corresponds to the reference simulation. The dashed line corresponds to a simulation in which only liquid PSCs were allowed. The dash-dotted line corresponds to a simulation in which NAT is formed at the NAT equilibrium temperature.

simulated chemical ozone loss for different assumptions as a function of equivalent latitude (as in Figure 6). The solid line shows the standard case, that is, NAT formation at a supersaturation of HNO_3 over NAT of 10. The dashed line corresponds to a simulation in which only liquid ternary aerosol and no NAT formation was allowed. The dash-dotted line corresponds to a simulation with NAT formation directly at the NAT equilibrium temperature. From Figure 12 it can be seen that the sensitivity to the particle formation assumptions is low: the difference in chemical ozone depletion between the different assumptions is 0.1 ppm at most.

5.4. Comparison With Triple Measurements

[39] The CLaMS simulation was also compared with the ClO measurements on board the Triple gondola flight on 1 March. As above, backward trajectories to the previous day 1200 UTC were calculated, along which the chemistry was then integrated. Figure 13 displays the simulated ClO mixing ratio at the balloon's location between the 400 and 475 K isentrope. During the night (balloon ascent) the simulation overestimates the ClO mixing ratio by about 50 ppt. The daylight observations of ClO are well reproduced within the error bars, although some of the vertical fine structure is missing due to the height resolution of this simulation. In the ER-2 flight level around 450 K, the simulation underestimates the ClO mixing ratio in contrast to the comparison with the ER-2 data. The reason for the difference in the comparison with the two data sets is still unclear and needs further investigation.

6. Summary and Conclusions

[40] A CLaMS simulation for mid February to mid March 2000 was performed initialized from a variety of different data sets. For this period, significant chemical ozone destruction of 1.6 ppm was found for the 425 and 450 K isentropes in the core region of the polar vortex. The maximum vortex-averaged chemical ozone loss rates were of the order of 50 ppb d^{-1} or 4 ppb per sunlight hour in early March. Compared with results from the Match technique using the same vortex definitions, the simulation underestimates the ozone depletion rate by 20–30%. With the tighter vortex definition [*Nash et al.*, 1996] used here, the results of the simulations agree with the Match results pointing to possible discrepancies in the vortex edge region between the two studies. The results of the simulations were compared with in situ measurements on board the ER-2 aircraft and the Triple balloon gondola. Comparisons with ER-2 measurements of ozone and NO_y outside the polar vortex show good agreement indicating correct initialization and transport of the simulation. The simulated ozone mixing ratios below the 450 K level also show good agreement with ER-2 measurements. Thus the ozone depletion deduced from the comparison with the simulated passive ozone tracer is reproduced correctly below the 450 K level. Above 450 K the simulation underestimates the ozone depletion. This is likewise seen by comparing the results of the simulation with estimates of ozone depletion from other sources. This problem may be due to inaccuracies in the tracer initialization because fewer data sources were available at the 475 K level. One other possible cause may be the underestimation of ozone depletion rates in early February as has also been found for previous winters at 475 K and above [see, e.g., *Becker et al.*, 1998, 2000b; *Woyke et al.*, 1999]. Open questions still remain regarding the comparison of the simulation of active chlorine species with the ER-2 observations. The CLaMS results underestimate daytime ClO above 430 K compared with the Triple balloon measurements but remain within the measurement uncertainty. In contrast, CLaMS overestimates the active chlorine measurements made on board the ER-2. If the lower levels

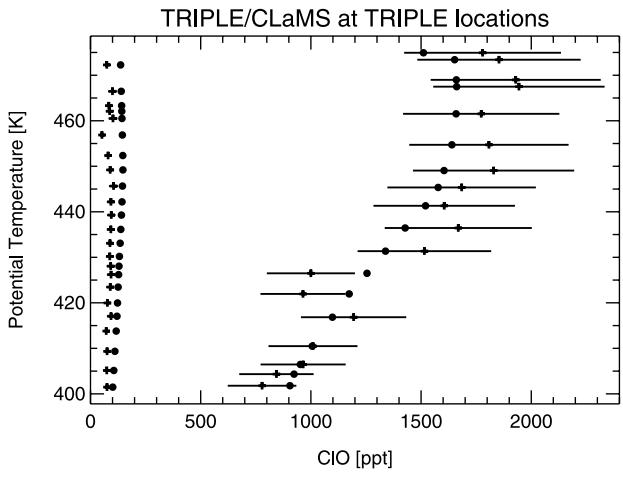

Figure 13. ClO comparison of the Triple measurements with the CLaMS simulation at the balloon's locations. Shown is the simulated (circles) and measured (pluses) ClO mixing ratio from the 1 March flight. The profile of low values (<200 ppt) corresponds to the ascent in darkness (solar zenith angle <96°), and the other points correspond to the descent profile in daylight (solar zenith angle ≈80°).

of active chlorine as observed on board the ER-2 were reproduced in the model simulations, this would result in a lower simulated ozone depletion. Further, the simulations indicate that most denitrification already occurred during January. The denitrification had a strong impact on chlorine deactivation and ozone depletion starting in early March. By 20 March the simulations indicate an enhanced ozone depletion of 0.3 ppm compared with simulations without denitrification.

[41] **Acknowledgments.** The authors gratefully acknowledge the enormous effort associated with the measurements and the permission to use the data gathered by various groups, especially David W. Fahey (NOAA) for the NO_y data and Richard Stimpfle (Harvard University) for the ClO, Cl_2O_2, and $ClONO_2$ data on board the ER-2 flights, James M. Russell (Hampton University) for the HALOE data and the European Centre for Medium-Range Weather Forecasts (ECMWF) for the meteorological analysis data. Ross Salawitch (JPL) provided the very useful time-synchronized data sets for the ER-2 flights. The authors thank the three anonymous referees for their constructive comments. Peter Popp (NOAA) provided the NO_y*/N_2O correlation prior to publication. The CH_4 measurements in the cryogenic whole air samples were performed by Ingeborg Levin (University of Heidelberg). We also acknowledge fruitful discussions with James C. Wilson (Denver University). This work was funded by the European Union under contract EVK2-1999-00311.

References

Becker, G., R. Müller, D. S. McKenna, M. Rex, and K. S. Carslaw, Ozone loss rates in the Arctic stratosphere in the winter 1991/92: Model calculations compared with Match results, *Geophys. Res. Lett.*, *25*, 4325–4328, 1998.

Becker, G., J.-U. Grooß, D. S. McKenna, and R. Müller, Stratospheric photolysis frequencies: Impact of an improved numerical solution of the radiative transfer equation, *J. Atmos. Chem.*, *37*, 217–229, 2000a.

Becker, G., R. Müller, D. S. McKenna, M. Rex, K. S. Carslaw, and H. Oelhaf, Ozone loss rates in the Arctic stratosphere in the winter 1994/1995: Model simulations underestimate results of the Match analysis, *J. Geophys. Res.*, *105*, 15,175–15,184, 2000b.

Brune, W. H., J. G. Anderson, and K. R. Chan, In situ observations of ClO in the Antarctic: ER-2 aircraft results from 54°S to 72°S latitude, *J. Geophys. Res.*, *94*, 16,649–16,663, 1989.

Carslaw, K. S., B. P. Luo, and T. Peter, An analytical expression for the composition of aqueous HNO_3-H_2SO_4-H_2O stratospheric aerosols including gas phase removal of HNO_3, *Geophys. Res. Lett.*, *22*, 1877–1880, 1995.

Carver, G. D., and P. A. Scott, IMPACT: An implicit time integration scheme for chemical species and families, *Ann. Geophys.*, *18*, 337–346, 2000.

DeMore, W. B., S. P. Sander, D. M. Golden, R. F. Hampson, M. J. Kurylo, C. J. Howard, A. R. Ravishankara, C. E. Kolb, and M. J. Molina, Chemical kinetics and photochemical data for use in stratospheric modeling, *JPL Publ.*, *97-4*, 1997.

Elkins, J. W., et al., Airborne gas chromatograph for in situ measurements of long-lived species in the upper troposphere and lower stratosphere, *Geophys. Res. Lett.*, *23*, 347–350, 1996.

Fahey, D. W., K. K. Kelly, G. V. Ferry, L. R. Poole, J. C. Wilson, D. M. Murphy, M. Loewenstein, and K. R. Chan, In situ measurements of total reactive nitrogen, total water, and aerosol in a polar stratospheric cloud in the Antarctic, *J. Geophys. Res.*, *94*, 11,299–11,315, 1989.

Fahey, D. W., et al., The detection of large HNO_3-containing particles in the winter Arctic stratosphere, *Science*, *291*, 1026–1031, 2001.

Gidel, L. T., P. J. Crutzen, and J. Fishman, A two-dimensional photochemical model of the atmosphere, 1, Chlorocarbon emissions and their effect on stratospheric ozone, *J. Geophys. Res.*, *88*, 6622–6640, 1983.

Grooß, J.-U., Modelling of stratospheric chemistry based on HALOE/UARS satellite data, Ph.D. thesis, Univ. of Mainz, Mainz, Germany, 1996.

Hansen, G., T. Svenøe, M. P. Chipperfield, A. Dahlback, and U.-P. Hoppe, Evidence of substantial ozone depletion in winter 1995/96 over northern Norway, *Geophys. Res. Lett.*, *24*, 799–802, 1997.

Hoppel, K., et al., POAM III observations of arctic ozone loss for the 1999/2000 winter, *J. Geophys. Res.*, *107*, 10.1029/2001JD000476, in press, 2002.

Konopka, P., J.-U. Grooß, G. Günther, D. S. McKenna, R. Müller, J. W. Elkins, D. Fahey, P. Popp, and R. M. Stimpfle, Weak influence of mixing on the chlorine deactivation during SOLVE/THESEO-2000: Lagrangian modeling (CLaMS) versus ER-2 in situ observations, *J. Geophys. Res.*, *107*, 10.1029/2001JD000876, in press, 2002.

Lary, D. J., and J. A. Pyle, Diffuse radiation, twilight, and photochemistry, I, *J. Atmos. Chem.*, *13*, 373–406, 1991.

Lucke, R. L., et al., The Polar Ozone and Aerosol Measurement (POAM) III instrument and early validation results, *J. Geophys. Res.*, *104*, 18,785–18,799, 1999.

Manney, G. L., and J. L. Sabutis, Development of the polar vortex in the 1999–2000 Arctic winter stratosphere, *Geophys. Res. Lett.*, *27*, 2589–2592, 2000.

McKenna, D. S., P. Konopka, J.-U. Grooß, G. Günther, R. Müller, R. Spang, D. Offermann, and Y. Orsolini, A new Chemical Lagrangian Model of the Stratosphere (CLaMS), 1, Formulation of advection and mixing, *J. Geophys. Res.*, *107*, 4309, doi:10.1029/2000JD000114, 2002a.

McKenna, D. S., J.-U. Grooß, G. Günther, P. Konopka, R. Müller, and G. Carver, A new Chemical Lagrangian Model of the Stratosphere (CLaMS), 2, Formulation of chemistry scheme and initialization, *J. Geophys. Res.*, *107*, 4256, doi:10.1029/2000JD000113, 2002b.

Morcrette, J.-J., Radiation and cloud radiative properties in the European Centre for Medium-Range Weather Forecasts forecasting system, *J. Geophys. Res.*, *96*, 9121–9132, 1991.

Nash, E. R., P. A. Newman, J. E. Rosenfield, and M. R. Schoeberl, An objective determination of the polar vortex using Ertel's potential vorticity, *J. Geophys. Res.*, *101*, 9471–9478, 1996.

Pierson, J. M., K. A. McKinney, D. W. Toohey, J. Margitan, U. Schmidt, A. Engel, and P. A. Newman, An investigation of ClO photochemistry in the chemically perturbed Arctic vortex, *J. Atmos. Chem.*, *32*, 61–81, 1999.

Popp, P. J., et al., Severe and extensive denitrification in the 1999–2000 Arctic winter stratosphere, *Geophys. Res. Lett.*, *28*, 2875–2878, 2001.

Proffitt, M. H., and R. J. McLaughlin, Fast-response dual-beam UV absorption ozone photometer suitable for use on stratospheric balloons, *Rev. Sci. Instrum.*, *54*, 1719–1728, 1983.

Rex, M., et al., Chemical depletion of Arctic ozone in winter 1999/2000, *J. Geophys. Res.*, *107*, 10.1029/2001JD000533, in press, 2002.

Richard, E. C., et al., Severe chemical ozone loss in the Arctic polar vortex during winter 1999–2000 inferred from in situ airborne measurements, *Geophys. Res. Lett.*, *28*, 2197–2200, 2001.

Robinson, A., et al., Ozone loss derived from balloon-borne tracer measurements and the SLIMCAT CTM, *J. Geophys. Res.*, *107*, in press, 2002.

Romashkin, P. A., D. F. Hurst, J. W. Elkins, G. S. Dutton, D. W. Fahey, R. E. Dunn, F. L. Moore, R. C. Myers, and B. D. Hall, In situ measurements of long-lived trace gases in the lower stratosphere by gas chromatography, *J. Atmos. Oceanic Technol.*, *18*(7), 1195–1204, 2001.

Russell, J. M., L. L. Gordley, J. H. Park, S. R. Drayson, A. F. Tuck, J. E. Harries, R. J. Cicerone, P. J. Crutzen, and J. E. Frederick, The Halogen Occultation Experiment, *J. Geophys. Res.*, *98*, 10,777–10,797, 1993.

Sander, S. P., et al., Chemical kinetics and photochemical data for use in stratospheric modeling; Supplement to evaluation 12: Update of key reactions, *JPL Publ.*, *00-3*, 2000.

Schauffler, S. M., E. L. Atlas, D. R. Blake, F. Flocke, R. A. Lueb, J. M. Lee-Taylor, V. Stroud, and W. Travnicek, Distributions of brominated organic compounds in the troposphere and lower stratosphere, *J. Geophys. Res.*, *104*, 21,513–21,536, 1999.

Schiller, C., et al., Dehydration in the Arctic stratosphere during the SOLVE/THESEO-2000 campaigns, *J. Geophys. Res.*, *107*, 10.1029/2001JD000463, in press, 2002.

Schmidt, U., G. Kulessa, E. Klein, E. P. Roeth, P. Fabian, and R. Borchers, Intercomparison of balloon-borne cryogenic whole air samplers during the MAP/GLOBUS 1983 campaign, *Planet. Space Sci.*, *35*, 647–656, 1987.

Seinfeld, J. H., and S. N. Pandis, *Atmospheric Chemistry and Physics*, John Wiley, New York, 1998.

Sinnhuber, B.-M., et al., Large loss of total ozone during the Arctic winter of 1999/2000, *Geophys. Res. Lett.*, *27*, 3473–3476, 2000.

Stimpfle, R. M., et al., The coupling of $ClONO_2$, ClO, and NO_2 in the lower stratosphere from in situ observations using the NASA ER-2 aircraft, *J. Geophys. Res.*, *104*, 26,705–26,714, 1999.

Vogel, B., et al., Vertical profiles of activated ClO and ozone loss in the Arctic vortex in January and March 2000: In situ observations and model simulations, *J. Geophys. Res.*, *107*, doi:10.1029/2002JD002564, in press, 2002.

Webster, C. R., R. May, C. A. Trimble, R. G. Chave, and J. Kendall, Aircraft laser infrared absorption spectrometer (ALIAS) for in situ atmospheric measurements of HCl, N_2O, CH_4, NO_2, and HNO_3, *Appl. Opt.*, *33*, 454–472, 1994.

Woyke, T., R. Müller, F. Stroh, D. S. McKenna, A. Engel, J. J. Margitan, M. Rex, and K. S. Carslaw, A test of our understanding of the ozone chemistry in the Arctic polar vortex based on in situ measurements of ClO,

BrO, and O_3 in the 1994/1995 winter, *J. Geophys. Res.*, *104*, 18,755–18,768, 1999.

Zhong, W., and J. D. Haigh, Improved broadband emissivity parameterization for water vapor cooling rate calculations, *J. Atmos. Sci.*, *52*, 124–138, 1995.

D. G. Baumgardner, Centro de Ciencias de la Atmosfera, Universidad Nacional Autonoma de Mexico, 04510 Mexico City, Mexico. (darrel@servidor.unam.mx)

R. Bevilacqua and K. Hoppel, Naval Research Laboratory, MC 4138BE Washington, DC 20375, USA. (bevilacqua@nrl.navy.mil)

J.-U. Grooß, G. Günther, P. Konopka, D. S. McKenna, R. Müller, F. Stroh, and B. Vogel, Forschungszentrum Jülich, Institute for Stratospheric Chemistry (ICG-1), 52425 Jülich, Germany. (j.-u.grooß@fz-juelich.de)

J. W. Elkins, D. F. Hurst, and P. A. Romashkin, Climate Monitoring and Diagnostics Laboratory, NOAA, Boulder, CO, USA. (James.W.Elkins@noaa.gov; dhurst@cmdl.noaa.gov; Pavel.Romashkin@noaa.gov)

A. Engel and M. Müller, Institute for Meteorology, University of Frankfurt, 60325 Frankfurt, Germany. (an.engel@meteor.uni-frankfurt.de; m.mueller@meteor.uni-frankfurt.de)

E. Richard, Aeronomy Laboratory, NOAA, 325 Broadway, Boulder, CO 80303, USA. (richard@al.noaa.gov)

C. R. Webster, Jet Propulsion Laboratory, California Institute of Technology, 4800 Oak Grove Dr., MS 183-301, Pasadena, CA 91109, USA. (Chris.R.Webster@jpl.nasa.gov)